JBC RESEARCH ARTICLE

Iron accumulation with age alters metabolic pattern and circadian clock gene expression through the reduction of AMP-modulated histone methylation

Received for publication, March 20, 2022, and in revised form, April 14, 2022 Published, Papers in Press, April 20, 2022,
https://doi.org/10.1016/j.jbc.2022.101968

Junhao Liu[1,‡], **Yang Zhao**[1,‡], **Zhao Ding**[1], **Yue Zhao**[2], **Tingting Chen**[1], **Wenhao Ge**[1], **and Jianfa Zhang**[1,*]

From the [1]*Center for Molecular Metabolism, Nanjing University of Science & Technology, Nanjing, China;* [2]*Institute of Molecular and Cell Biology, Agency for Science, Technology and Research (A*STAR), Singapore*

Edited by Ruma Banerjee

Iron accumulates with age in mammals, and its possible implications in altering metabolic responses are not fully understood. Here, we report that both high-iron diet and advanced age in mice consistently altered gene expression of many pathways, including those governing the oxidative stress response and the circadian clock. We used a metabolomic approach to reveal similarities between metabolic profiles and the daily oscillation of clock genes in old and iron-overloaded mouse livers. In addition, we show that phlebotomy decreased iron accumulation in old mice, partially restoring the metabolic patterns and amplitudes of the oscillatory expression of clock genes *Per1* and *Per2*. We further identified that the transcriptional regulation of iron occurred through a reduction in AMP-modulated methylation of histone H3K9 in the *Per1* and H3K4 in the *Per2* promoters, respectively. Taken together, our results indicate that iron accumulation with age can affect metabolic patterns and the circadian clock.

Iron is a vital trace element for most organisms, and it functions in numerous physiological processes. In mammalian cells, iron is an essential substrate for the biosynthesis of heme and sulfur–iron cluster proteins (1). Iron deficiency could lead to disorders including but not limited to anemia (2), and excess iron is damaging since iron is highly reactive and able to generate reactive oxygen species (ROS), which promote peroxidation and oxidative stress (3). Aberrant iron accumulation is frequently observed in chronic liver diseases, such as alcoholic liver disease, nonalcoholic fatty liver disease, and steatohepatitis (4). Iron overload has been implicated for enhancing age-related diseases, such as developing diabetes, inducing tumorigenesis, and accelerating cancer progression (5–8).

Iron homeostasis is commonly considered regulated by iron absorption since it is traditionally thought that there are no mechanisms of iron excretion. However, recent work has challenged this notion. Mercadante *et al.* (9) reported that transferrin (Tf) treatment increased iron excretion through gastrointestine in Tf-deficient iron-overload mice. And under the condition of dietary iron overload, excess iron could be partly excreted through bile (10). Although iron excretion is significantly elevated, it is still not enough to reverse iron overload completely in both cases. In addition, there are also very small quantities eliminated *via* urine, sweating, and shedding of epidermal cells (11). Iron absorption is mainly from the proximal duodenum (12). Non-heme iron is transported into enterocytes by divalent metal transporter 1 after being reduced to Fe^{2+} (12, 13). However, the mechanisms for intestinal heme iron import are largely unknown. While the folate transporter, heme carrier protein 1, has previously been implicated as a low-affinity heme uptake system, its physiological significance in dietary heme import is controversial (14). Iron absorption is regulated by hepcidin, a key iron-regulating peptide secreted predominantly by hepatocytes (15).

Iron accumulates during aging, which has been proved by previous studies (16). Massie *et al.* (17) demonstrated that total iron contents in the liver, brain, kidney, and heart were dramatically higher in aged male C57BL/6J mice compared with young ones. Sohal *et al.* (18) revealed an increase of non-heme iron concentration in the liver, kidney, heart, and brain. Especially, bleomycin-chelatable iron (redox-active iron) in the liver was specifically increased with age. In addition, caloric restriction was reported to alleviate iron accumulation with age in multiple tissues (19, 20). High-iron diets have been used to create iron-overload models to investigate the effects caused by excess iron (21). Oxidative stress occurs in iron overload, with the decreased antioxidants and the increase in ROS (21, 22). Aging is related to increases of oxidative stress in the liver and other tissues (23–25). Increasing oxidative stress has been implicated with age-related changes in circadian function and sleep quality (26–28). Iron overload has also frequently induced mice into sleep disturbances and obvious shifts in the daily rhythms of locomotor activity (29–31).

In the present study, we demonstrated that iron accumulation is a major cause of age-related changes in metabolic patterns and circadian clock. We uncovered a mechanism by which iron reciprocally regulates *Per1* and *Per2* transcription through histone demethylation. At last, we presented that blood donation or phlebotomy is a feasible strategy to prevent

‡ These authors contributed equally to this work.
* For correspondence: Jianfa Zhang, jfzhang@njust.edu.cn.

the detrimental effects caused by accumulating iron during aging.

Results

Age-dependent iron accumulations

We first compared the iron content in serum and livers of young mice at 8 weeks and old mice at 64 weeks. We found that serum iron and Tf saturation in old mice were significantly higher, accompanied by lower unbound iron-binding capacity with total iron-binding capacity unchanged (Fig. 1*A*). Diaminobenzidine (DAB)-enhanced Prussian blue staining of livers from old mice showed more extensive stainable iron compared with that in young mice (Fig. 1*B*). Quantitative measurement of iron in the liver confirmed an increase of iron accumulation with age (Fig. 1*C*). The significant increases in iron accumulation with age were also observed in other organs, including the heart, kidney, brain, and spleen (Fig. S1). Moreover, excess iron supplement to young mice also led to elevated serum iron and Tf saturation (Fig. 1*D*), exhibiting a significantly higher accumulation of iron in livers (Fig. 1, *E* and *F*) and other peripheral organs (Fig. S2). These results indicated that iron was inevitably accumulated in the tissues with age because of the imbalance of iron intake and excretion.

Iron accumulations change the general profiles of gene expression

To analyze the physiological association between iron accumulation and aging, RNA-Seq was performed to analyze

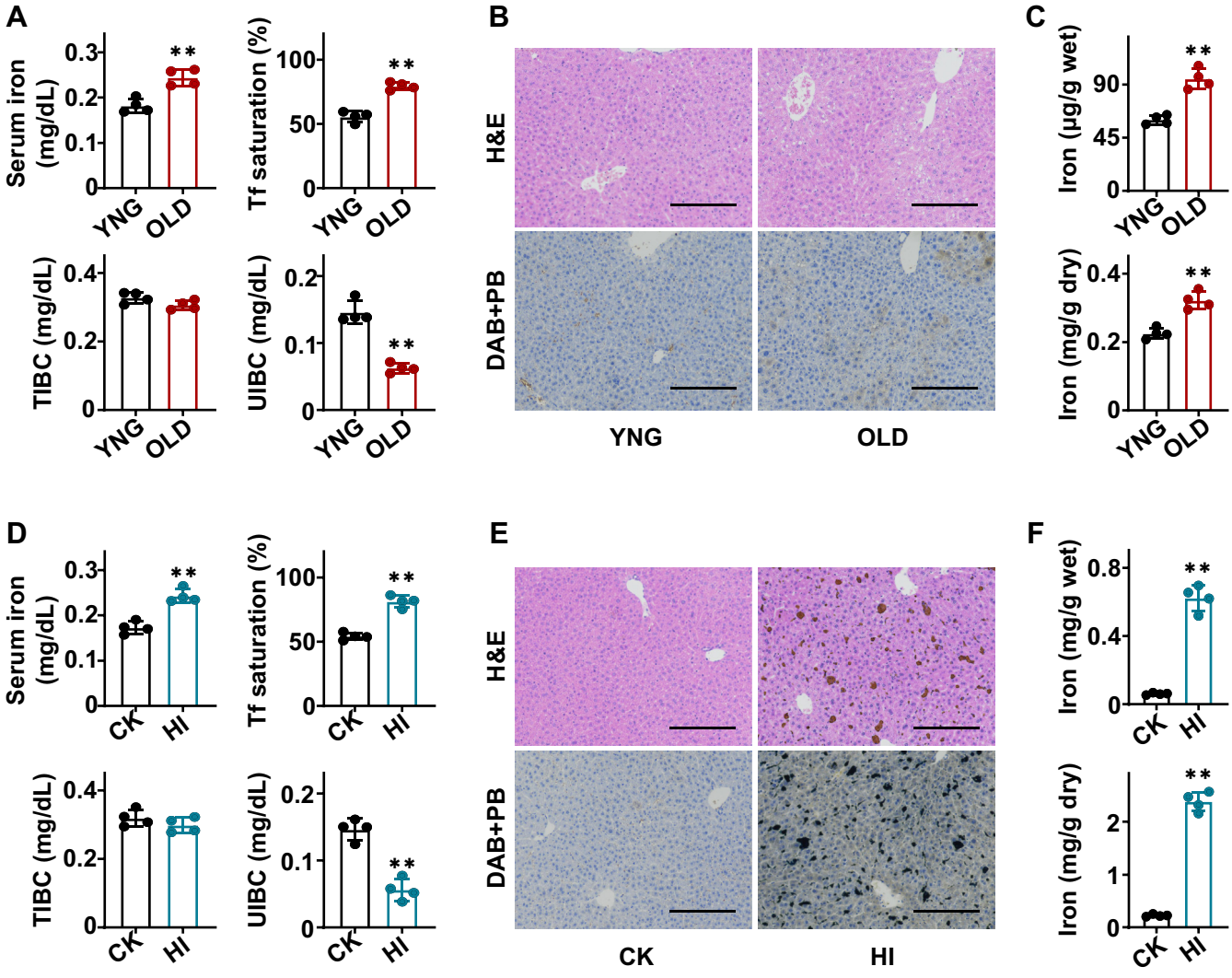

Figure 1. Imbalance of iron intake and excretion causes iron accumulation with age. *A*, serum iron levels, transferrin (Tf) saturation, total iron-binding capacity (TIBC), and unbound iron-binding capacity (UIBC) in young (8 weeks old) and old (64 weeks old) mice. OLD, old group (n = 4); YNG, young group. *B*, representative H&E staining and DAB-enhanced Prussian staining of liver sections of young and old mice (n = 4; the scale bars represent 200 μm). *C*, liver iron content in young and old mice. Data are expressed as iron (μg)/liver wet weight (g) and iron (mg)/liver dry weight (g), respectively (n = 4). *D*, serum iron levels, Tf saturation, TIBC, and UIBC in control and iron-overload mice. Iron overload was induced by i.p. injection of iron dextran (5 mg/mouse/day) twice a week for 3 weeks. CK, control group; HI, iron-overload group (n = 4). *E*, representative H&E staining and DAB-enhanced Prussian staining of liver sections of control and iron-overload mice (n = 4; the scale bars represent 200 μm). *F*, liver iron content in control and iron-overload mice. Data were expressed as iron (μg)/liver wet weight (g) and iron (mg)/liver dry weight (g), respectively (n = 4). All data are expressed as the means ± SD, $*p < 0.05$, $**p < 0.01$. Four-week-old male C57BL/6 mice were used to induce iron overload by i.p. injection of iron dextran (5 mg/mouse/day) twice a week for 3 weeks, and mice were sacrificed 1 week after the last injection. And 64-week-old male mice were used for the old group. DAB, diaminobenzidine.

all poly A-containing transcripts in the livers of old mice and iron-overload mice. Using the Kyoto Encyclopedia of Genes and Genomes (KEGG) database, the significantly enriched pathways were identified. Mapping of annotated differentially expressed genes (DEGs) to KEGG pathways revealed 947 DEGs and 666 DEGs of 34 pathways in the livers of iron-overload group (Fig. 2*A*, *left*) and old group (Fig. 2*A*, *right*), respectively. The 34 KEGG pathways were disturbed in both groups, implying that the transcription changes in iron-overload group have some degree of similarity to those seen in old group. The 450 genes that are markedly altered in the old group overlapped with those in the iron-overload group (Fig. 2*B*, *top*). The Venn diagram revealed 88 upregulated genes and 182 downregulated genes that were commonly modulated in both groups (Fig. 2*B*, *bottom*). A heatmap of the 450 genes with significant regulatory functions was constructed (Fig. 2*C*). Pearson *r* analysis showed that there was a strong correlation between biological repeats in each group. On the DEGs of aging pathway, the top 20 altered pathways in upregulated and downregulated genes were shown in Figure 2*D*. Most of the changed genes related to metabolic regulation and oxidative stress were consistently changed in both groups. Real-time RT–PCR analysis confirmed that increased *Maoa*, *Gpx3*, *Gadd45a*, *Plk2*, *Dapk2*, and *Cd36*, and decreased *Prdx5*, *Gpx1*, *Gstm2*, *Gstp1*, *Ulk2*, and *Gsto1* in old and iron-overload groups (Fig. 2*E*), and these target genes with meaningfully changed expression, were concerned with oxidative stress. Together, these results revealed a possibility that age-increased oxidative stress is partially contributed by the iron accumulation with age.

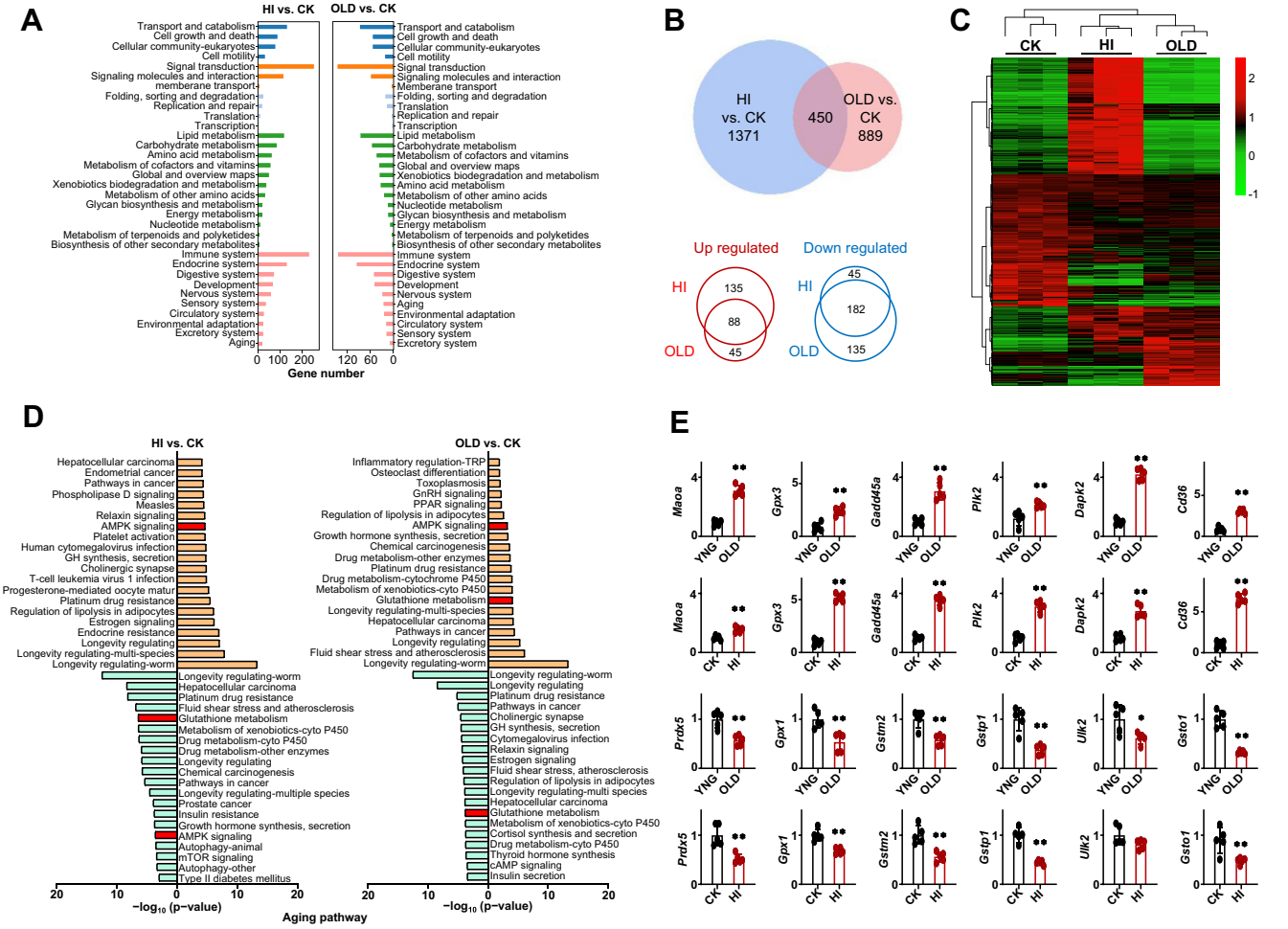

Figure 2. RNA-Seq analysis of old and iron-overload mice. *A*, distribution of the KEGG pathways at level 2 in the livers of old mice and iron-overload mice induced by iron dextran, respectively. The bar chart showed the numbers of sequences within different pathway categories. CK, control group; HI, iron overload group; OLD, old group (n = 3). *B*, Venn diagram illustrating the extent of overlap among the differentially expressed genes (DEGs) observed in each group. The 450 genes regulated in the iron-overload mice significantly overlapped with the same genes in old mice (*upper*). Venn diagram for upregulated genes or downregulated genes among the overlapped 450 genes was shown (*down*). *C*, heatmap representation of 450 overlapping genes in old and iron-overload mice. *D*, KEGG significant enrichment analysis for the aging pathway. Top 20 most significantly altered pathways in aging pathway mapped with downregulated DEGs and upregulated DEGs in HI group compared with CK group (*left*). Top 20 most significantly altered pathways in aging pathway mapped with downregulated DEGs and upregulated DEGs in OLD group compared to CK group (*right*). *Red bars* indicated the same changed pathways related to oxidative stress between HI and OLD groups. *E*, real-time PCR analysis for mRNA expression of genes related to oxidative stress in old and iron-overload mice. CK, control group; HI, iron-overload group; OLD, old group; YNG, young group. All data are expressed as the means ± SD (*$p < 0.05$, **$p < 0.01$, n = 5). Four-week-old male C57BL/6 mice were used to induce iron overload by i.p. injection of iron dextran (5 mg/mouse/day) twice a week for 3 weeks, and mice were sacrificed 1 week after the last injection. And 64-week-old male mice were used for the old group. KEGG, Kyoto Encyclopedia of Genes and Genomes.

Iron accumulation and circadian clock

Iron accumulations shift metabolic patterns

To characterize the metabolic changes of iron-related aging, we acquired ^{1}H NMR-based metabonomics analysis on old mice and iron-overload mice. As a metabolic profiling technique, metabonomics analysis allowed us to acquire the small-molecule metabolite profiles and analyze the differences in the metabolic profiles between groups. The orthogonal partial least squares discriminant analysis (OPLS-DA) score plots of control and old groups were distinct (Fig. 3*A*, *left*), and a clear separation was observed between control group and iron-overload groups as well (Fig. 3*B*, *left*). The corresponding loading plots displayed similar patterns (Fig. 3*A*, *right*; Fig. 3*B*, *right*). The identified metabolites from the NMR data of all groups were shown as a heatmap in Figures 3*C*, S3, and Table S1. The metabolite changes in iron-overload group were highly similar to that observed in old group. The identified metabolites data were subject to pathway enrichment analysis, and many pathways were consistently altered in both groups, including glutathione, porphyrin and chlorophyll metabolism, glyoxylate and dicarboxylate metabolism, pantothenate and CoA biosynthesis, and others (Fig. 3*D*). OPLS-DA models were validated by permutation tests repeated 200 times for confirming the reliability (Fig. 3, *E* and *F*). In the principal component analysis score plot, old group and iron-overload group were both well separated from control group, whereas the old group overlapped with iron-overload group (Fig. 3*G*), suggesting similar metabolic changes in both groups. The scree plot showed the variance of the first five principal components (Fig. 3*H*), and it demonstrated that principal component 1 and principal component 2 were the most important ones as shown in Figure 3*G*. Next, hematology and biochemistry parameters related to oxidative stress and liver physiology were assessed. Both old and iron-overload groups showed noticeable increments in serum levels of aspartate aminotransaminase and alanine aminotransferase, hepatic malondialdehyde, accompanied by reduced antioxidant enzyme activities of superoxide dismutase, catalase (CAT), and GSH levels (Fig. 3*I*). These results further confirmed that age-related oxidative stress associates with iron accumulations with age.

Iron accumulations reset circadian clock

We also noted that environment adaptation pathway was obviously altered by pathway enrichment analysis in old and iron-overload groups, and circadian entrainment was one of the significantly disturbed pathways (Fig. 4*A*). To further confirm the results from RNA-Seq, we performed real-time RT–PCR analysis for clock genes in the livers of old and iron-overload mice. The mesor, amplitude, and acrophase of each fitting curve are listed in Tables S2 and S3. Unexpectedly, the alteration of core clock genes displayed broad similarity in old and iron-overload livers (Fig. 4, *B–M*). Specifically, a reciprocal change of *Per1* and *Per2* was observed in both groups, with elevated *Per1* expression and lowered *Per2* expression in both groups. These results implied that iron overload could contribute to the age-dependent shift in circadian function.

Phlebotomy partially restored the oscillation amplitudes of Per1 and Per2

To demonstrate that age-related iron accumulation was a key regulator in metabolism and circadian function, phlebotomy was applied to reduce iron stores, which is one of the most widely used methods to decrease systemic iron levels. Expectedly, serum iron and Tf saturation were decreased after phlebotomy (Fig. 5, *A–D*). Liver iron content was also reduced (Fig. 5*E*). H&E staining revealed nearly no morphological changes of the livers in phlebotomy groups. Nevertheless, DAB-enhanced Prussian blue staining demonstrated a decrease of iron accumulation in the livers after phlebotomy (Fig. 5*F*). The activities of superoxide dismutase and CAT were elevated by phlebotomy as well as GSH levels, and malondialdehyde levels were decreased (Fig. 5*G*). The ^{1}H NMR-based metabolome analysis confirmed that phlebotomy caused a significant recovery in the metabolic profiling. As shown in Figure 5,*H* and *I*, the metabolic profiles of young mice and old mice with phlebotomy were both well separated from that of old mice and close to each other. The corresponding loading plots and the alterations in identified metabolites also revealed high similarity between the metabolic profiles of young and old mice with phlebotomy (Fig. S6 and Table S4). The OPLS-DA models were validated with permutation tests (200 times) to confirm the reliability (Fig. 5*J*). The identified metabolites from the NMR data of all groups were shown as a heatmap in Figure 5*K*. Moreover, the mRNA expressions of antioxidant enzymes including *SOD1*, *SOD2*, *Gpx1*, and *CAT* were increased by phlebotomy in a dose-dependent manner (Fig. 5*L*). The oscillation amplitude of clock genes *Per1* and *Per2* was partially restored by phlebotomy (Fig. 5*M*). These results indicated that phlebotomy in old mice eliminated iron accumulation, restoring metabolic profiles and the clock function.

Iron accumulations increase intracellular ROS and AMP release in red blood cells

To show that iron directly functioned on *Per1* and *Per2* transcription, a luciferase reporter assay was used to examine the effects of iron on *Per1* and *Per2* transcription *in vitro*. Contrary to the assumption, iron with different concentrations did not significantly affect *Per1* and *Per2* transcription in cultural cells (Fig. 6*A*). However, mice that received i.v. injection with iron showed an increase of *Per1* expression and a decrease of *Per2* in livers, respectively, and the effect was in a time-dependent and dose-dependent manner (Fig. 6*B*). The aforementioned observations could be explained by a blood signal that acts as a modulator of *Per1* and *Per2* expression during iron injection, and iron is not the direct regulator. We reasoned that the putative regulator when injected into mice should induce changes of *Per1* and *Per2* expression instead of iron. The putative regulator could either be a peptide or an organic molecule, and we initially chose to analyze the latter

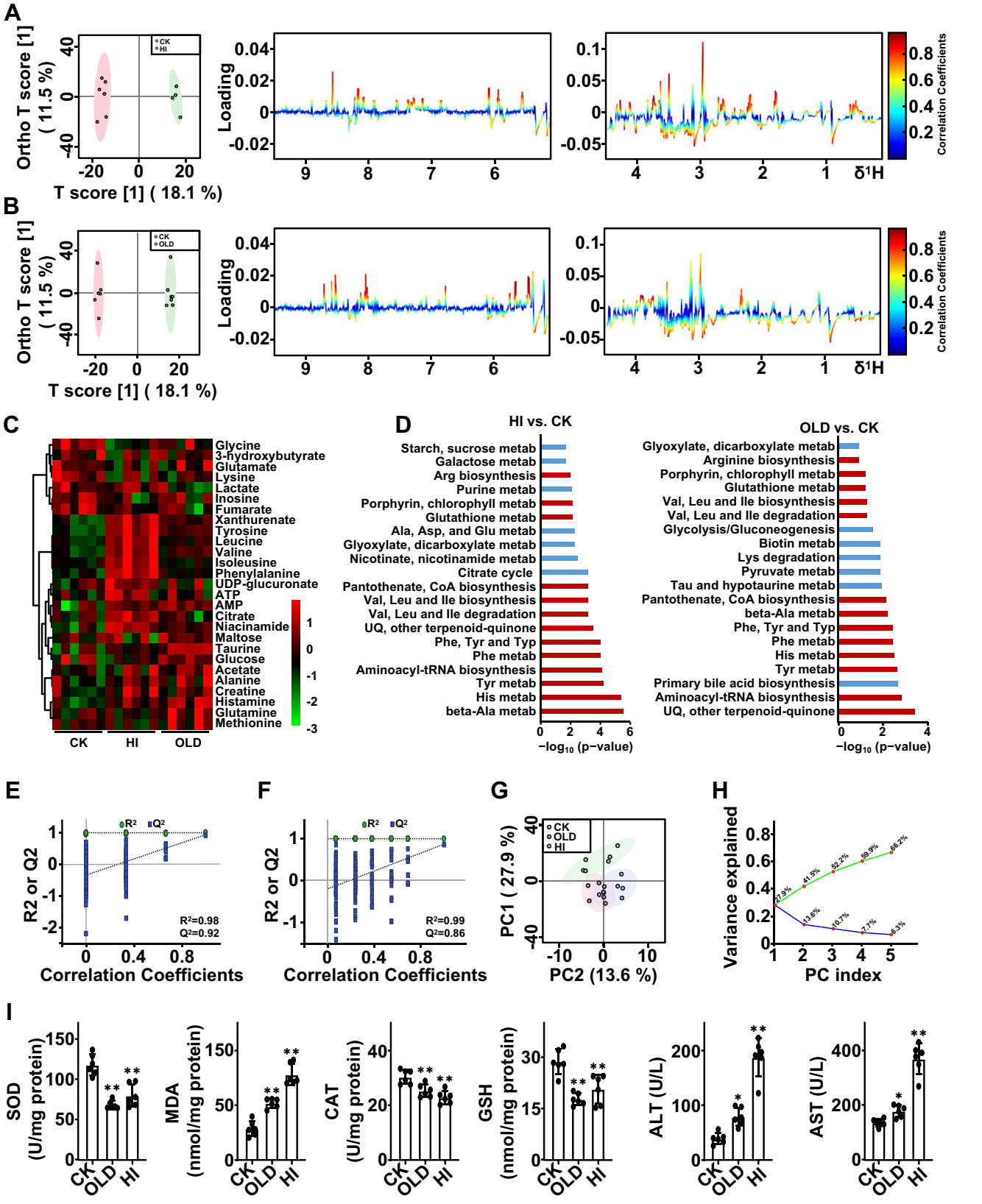

Figure 3. NMR-based metabonomics analysis of livers in old and iron-overload mice. *A*, score plot and loading plot from OPLS-DA analysis of the spectra from livers of the control mice and iron-overload mice (n = 6). *B*, score plot and loading plot from OPLS-DA analysis of the spectra from livers of the control mice and old mice (n = 6–7). *C*, heatmap visualization for liver samples from three groups. *D*, metabolite pathway enrichment analysis of iron-overload mice (*left*) and old mice (*right*) using data obtained by MetaboAnalyst 3.0. *Red bars* indicated the same changed metabolic pathways between HI and OLD groups. *E* and *F*, a 200 times permutation test of OPLS-DA models for iron-overload mice and old mice, respectively. *G*, PCA score plot of all three groups (n = 6–7). *H*, PCA scree plot showing the variance explained with the five principal components. The two *lines* stand for the individual (*bottom*) or

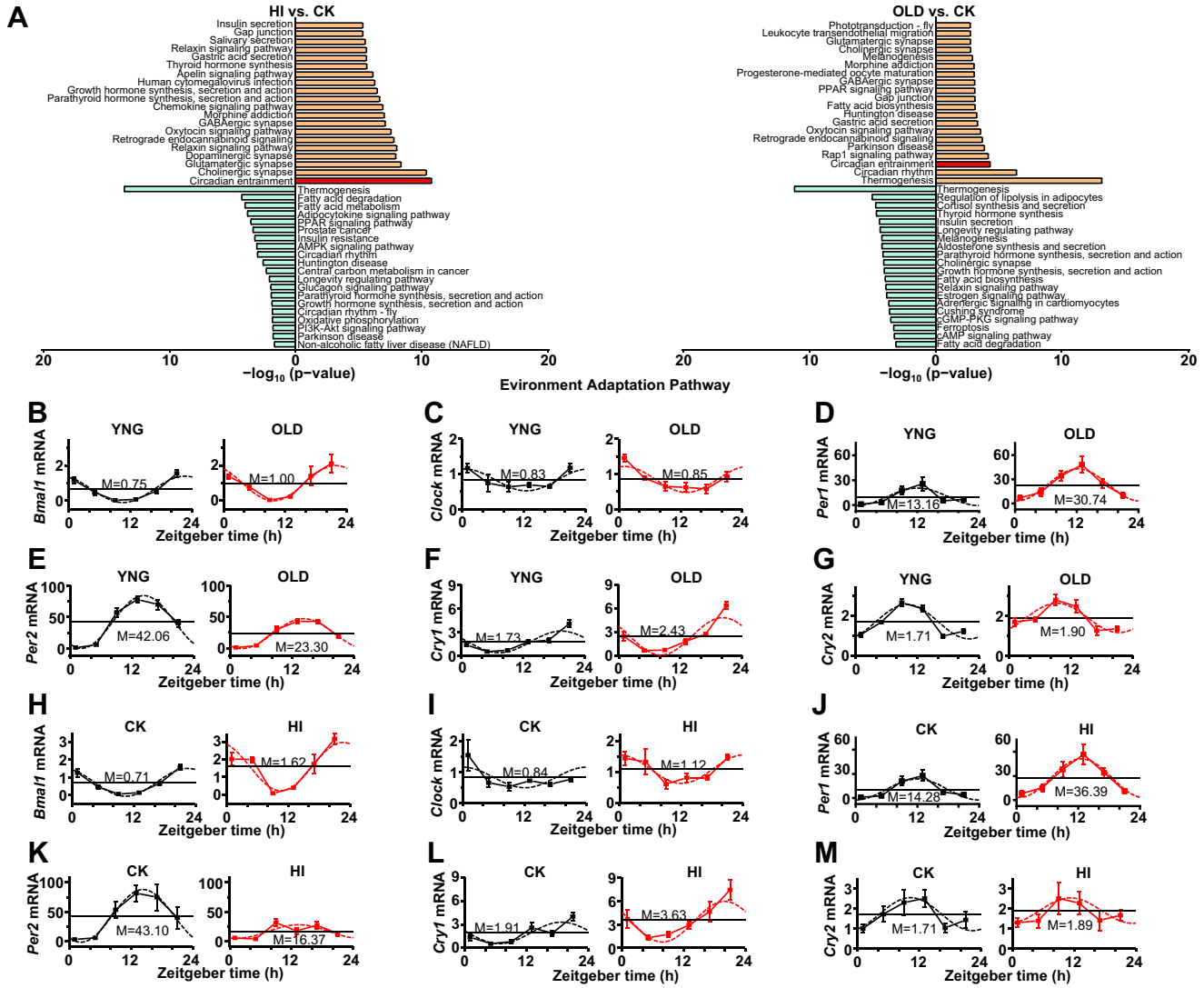

Figure 4. The similar variation of circadian gene expression in livers of old and iron-overload mice. *A*, KEGG significant enrichment analysis for the environment adaptation pathway. Top 20 altered pathways mapped with downregulated DEGs and upregulated DEGs in iron-overload mice (*left*). Top 20 altered pathways mapped with downregulated DEGs and upregulated DEGs in old mice. CK, control group; HI, iron overload group; OLD, old group (*right*). *Red bars* indicated an altered circadian pathway. Four-week-old male C57BL/6 mice were used to induce iron overload by i.p. injection of iron dextran (5 mg/mouse/day) twice a week for 3 weeks, and mice were sacrificed 1 week after the last injection. And 64-week-old male mice were used for the old group. Circadian expression of six core clock genes in the livers. Diurnal mRNA levels of (*B*) *Bmal1*, (*C*) *Clock*, (*D*) *Per1*, (*E*) *Per2*, (*F*) *Cry1*, and (*G*) *Cry2* were measured by real-time RT–PCR in livers of young (8 weeks old) and old (64 weeks old) mice. OLD, old group; YNG, young group. Diurnal mRNA levels of (*H*) *Bmal1*, (*I*) *Clock*, (*J*) *Per1*, (*K*) *Per2*, (*L*) *Cry1*, and (*M*) *Cry2* were measured by real-time PCR in livers of mice fed on normal chow diet (ND) or high-iron diet (HID) for 2 weeks from the age of 6 weeks. *Solid lines* represent experimental response curves; *dashed lines* indicate fit cosine curves. The *solid horizontal lines* indicate mesors. All data are presented as means ± SEM (n = 4 for each time point). DEG, differentially expressed gene; KEGG, Kyoto Encyclopedia of Genes and Genomes.

possibility. Plasma extracts obtained from mice with iron injection were analyzed with reverse-phase HPLC. The results revealed that iron injection caused an elevation of plasma AMP, and this effect was dose dependent (Fig. 6, *G* and *H*, *left*). An increased plasma AMP was also observed in old mice, and phlebotomy in old mice alleviated the elevation of plasma AMP (Fig. 6*H*, *right*). In isolated red blood cells (RBCs) and their lysates, iron significantly increased the total ROS levels (Fig. 6, *C–E*) with different levels. Iron-elevated ROS could induce hemolysis (Fig. 6*F*), which inevitably caused the release of intracellular nucleotides including AMP. To demonstrate that AMP is a regulator, we injected chemically synthesized AMP into mice to investigate whether clock gene expression was affected in the liver. Using quantitative RT–PCR analysis,

cumulative (*top*) variance explained by the principal components, respectively. *I*, liver oxidative stress and liver injury levels in livers of iron-overload and old mice. SOD activities, CAT activities, MDA levels, and GSH levels in livers, and serum AST and ALT levels were determined. Iron overload was induced by i.p. injection of iron dextran (5 mg/mouse/day) twice a week for 3 weeks, and 64-week-old male mice were used for the old group. All data are expressed as the means ± SD (*$p < 0.05$, **$p < 0.01$, n = 5). Four-week-old male C57BL/6 mice were used to induce iron overload by i.p. injection of iron dextran (5 mg/mouse/day) twice a week for 3 weeks, and mice were sacrificed 1 week after the last injection. And 64-week-old male mice were used for the old group. ALT, alanine aminotransferase; AST, aspartate aminotransaminase; CAT, catalase; HI, iron-overload group; MDA, malondialdehyde; OLD, old group; OPLS-DA, orthogonal partial least squares discriminant analysis; PCA, principal component analysis; SOD, superoxide dismutase.

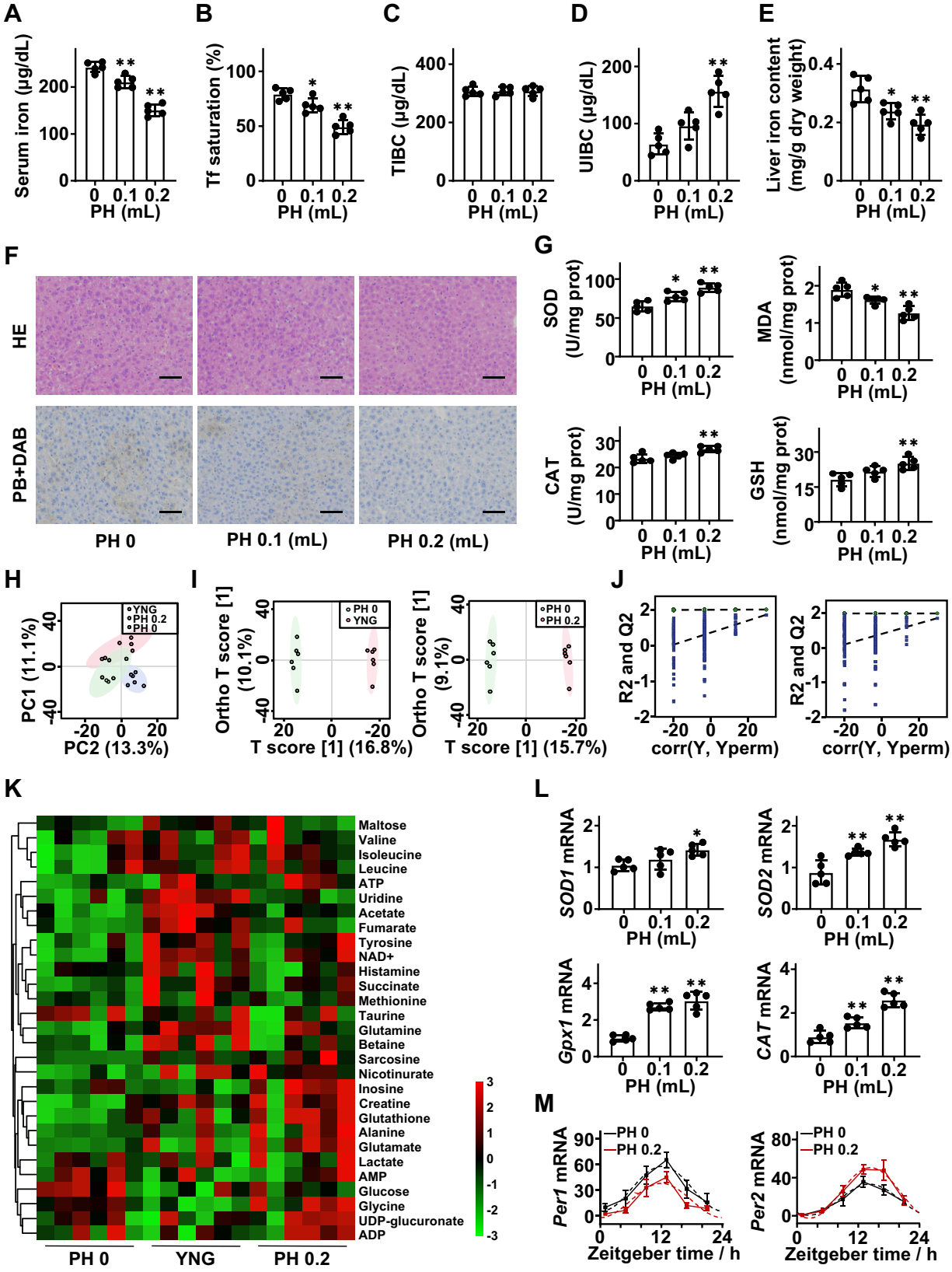

Figure 5. Phlebotomy partially restores metabolic profiles and the oscillation amplitudes of *Per1* and *Per2* in livers of old mice. *A*, serum iron, (*B*) Tf saturation, (*C*) TIBC, and (*D*) UIBC in old mice with phlebotomy. Phlebotomy was performed by 100 μl or 200 μl of bloodletting *via* cheek puncture. Mice were sacrificed 2 weeks after phlebotomy. PH, phlebotomy (n = 5). *E*, liver iron content in old mice with phlebotomy. Data were expressed as iron (mg)/liver dry weight (g) (n = 5). *F*, representative H&E staining and DAB-enhanced Prussian staining of liver sections of old mice with phlebotomy (n = 5; the scale bars represent 100 μM). *G*, effects of phlebotomy on the activities of liver SOD and CAT, and the level of liver MDA and GSH in old mice (n = 5). *H*, score plot from PCA analysis of the spectra from livers of young mice and old mice with or without 0.2 ml phlebotomy (n = 6). *I*, score plot from OPLS-DA analysis of

we could detect an increased *Per1* mRNA and a decreased *Per2* mRNA by AMP (Fig. 6*I*). Thus, these studies showed that AMP is a potential modulator by which iron regulates the expression of circadian genes.

A reciprocal regulation of Per1 *and* Per2 *transcription through AMP*

The extracellular nucleotidase converts AMP to adenosine in the plasma. Therefore, the most likely intracellular action of AMP would be *via* the adenosine receptors and transporter pathways. We injected adenosine into mice, and it also induced reciprocal changes of *Per1* and *Per2* expression (Fig. 7, *A* and *B*). Then we used NIH3T3 cells to explore the regulation effects of AMP. Theophylline, a nonspecific adenosine receptor antagonist, did not affect the AMP-induced changes of *Per1* and *Per2* expression (Fig. 7, *C* and *D*). An adenosine transporter inhibitor dipyridamole significantly inhibited the effect of AMP on *Per1* and *Per2* transcription (Fig. 7, *C* and *D*), indicating that the intracellular action of AMP is likely mediated through the adenosine transporter pathways. Moreover, AMP resulted in a significant decrease in the SAM/SAH ratio, a known cellular methylation potential (Fig. 7*E*). To further investigate whether cellular methylation potential is involved in the regulation of *Per1* and *Per2*, we used methylation activator SAM and methylation inhibitor cycloleucine to observe the effects on *Per1* and *Per2* transcription. While cycloleucine induced reciprocal changes of *Per1* and *Per2* transcription (Fig. 7*F*), the addition of SAM blocked the action of AMP (Fig. 7*G*). These results strongly suggest the axis of iron–ROS–AMP–methylation modulates clock gene expression. Then immunofluorescence analysis showed that AMP led to decreasing global H3K4me3 and H3K9me2 in a dose-dependent manner (Fig. 7,*H* and *I*), and the result was confirmed by Western blotting (Fig. 7*J*). Chromatin immunoprecipitation (ChIP) analysis revealed that AMP markedly decreased the abundance of H3K9me2 in the *Per1* promoter and did not affect H3K4me3 abundance. On the contrary, AMP decreased H3K4me3 abundance in *Per2* promoter with H3K9me2 abundance unchanged (Fig. 7, *K* and *L*). Similarly, we observed an elevated plasma level of AMP and a reciprocal change of histone methylation pattern in *Per1* and *Per2* promoters of old and iron-overload mice (Figs. S4 and S5). Together, our studies have identified that AMP is a signaling molecule that can regulate circadian function in response to disturbed iron homeostasis in old mice.

Discussion

Iron is one of the most abundant mineral elements in mammals and is obligatory for various essential metabolisms, including oxygen transport, and oxidative phosphorylation (32). Both iron deficiency and overload are associated with abnormal oxidative stress and elevated risks for diseases (33–36). Although a complex mechanism of regulating iron uptake has been evolved (37), mammals possess limited routes for iron excretion. In our present study, we highlighted that iron was inevitably accumulated in mouse tissues with age; iron accumulation with age resets metabolic patterns and the circadian clock in old mice.

It has not caused enough attentions that iron accumulation with age and possible implications for metabolic responses, because the concept of iron as an important essential nutrient, has been well known from the scientists to the public. Indeed, iron plays a decisive role in the growth and development of infants (38). Children who do not meet their iron needs *via* foods should receive a daily iron supplement (39). On the other hand, iron overload is also harmful to health (40, 41). Aging is accompanied by accumulated oxidative stress, which is thought to be one of the hallmarks of aging process (42). The oxidation products, such as protein carbonyls, 4-hydroxynonenal, and 8-hydroxy-2-deoxyguanosine, increase with age (43). Iron is an excellent catalyst that catalyzes free radical reactions for producing ROS (3). Young iron-overload mice showed a similar pattern to aging mice in the changing trend of metabolites. Thus, it is reasonable that iron accumulation should contribute, at least in part, to reprogram metabolic patterns during aging.

Aging is related to circadian rhythm disturbances, including irregular sleep–wake circadian disorder and advanced sleep phase syndrome (44). Iron accumulation must play a key role in aging-related shifts of circadian function, because iron supplement to young mice yields indistinguishable alterations of daily circadian gene expression from old mice. Especially, a reciprocal shift of the amplitude of *Per1* and *Per2* expression occurs in these mice. *Per1* and *Per2* are the core components of circadian clock pacemakers, which act as transcriptional repressors in the main transcriptional/translational feedback loop (45). The oscillation of hormone levels is weakened in old animals, indicating impaired circadian rhythms during aging (46–48). Aging is often accompanied by increased prevalence of sleep disturbances, and it has been estimated that about 50% of elderly people complain about poor sleep quality (49, 50). Sleep disturbances have been frequently seen in iron overload–related diseases (29, 30). Mice overloaded with iron exhibit disturbed locomotor activity rhythms (31). There have been some studies aiming to connect iron metabolism and circadian rhythms. Dietary iron was reported to affect circadian glucose production *via* heme synthesis (51). Heme modulates *Per1* and *Per2* expression in the liver of mice (52) and

the spectra from livers of the old mice compared with young mice (*left*) and old mice with 0.2 ml phlebotomy (*right*), respectively (n = 6). *J*, a 200 times permutation test of OPLS-DA models for old mice compared with young mice (*left*) and old mice with 0.2 ml phlebotomy (*right*), respectively (n = 6). *K*, heatmap visualization for liver samples of old mice with or without 0.2 ml phlebotomy (n = 6). *L*, effect of phlebotomy on the mRNA levels of antioxidant genes encompassing *SOD1*, *SOD2*, *Gpx1*, and *CAT* (n = 5). *M*, effect of phlebotomy on the diurnal oscillation of *Per1* and *Per2* mRNA levels. *Solid lines* represent experimental response curves; *dashed lines* indicate fit cosine curves (n = 4). All data are expressed as the means ± SD, $*p < 0.05$, $**p < 0.01$. CAT, catalase; DAB, diaminobenzidine; MDA, malondialdehyde; OPLS-DA, orthogonal partial least squares discriminant analysis; PCA, principal component analysis; SOD, superoxide dismutase; TIBC, total iron-binding capacity; Tf, transferrin; UIBC, unbound iron-binding capacity.

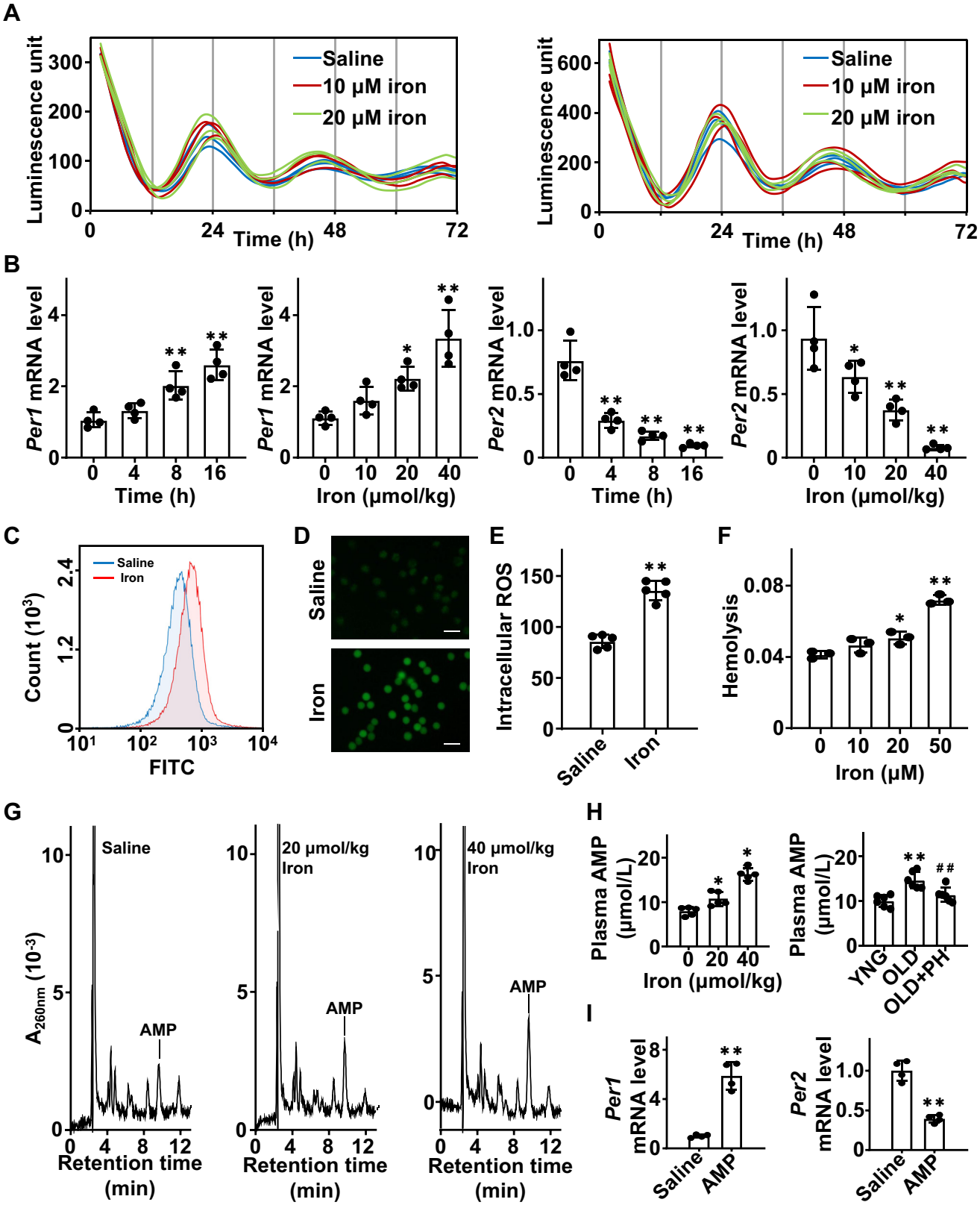

Figure 6. Iron induces the elevation of intracellular ROS and the release of AMP in RBCs. *A*, real-time bioluminescence recording of *Per1* (*left*) and *Per2* (*right*) oscillation in response to $FeSO_4$ at two different doses (10 and 20 μM) using *Per1*:Luc and *Per2*:Luc in NIH3T3 fibroblasts, respectively. $FeSO_4$ treatment did not have a significant change on *Per1* and *Per2* transcription (n = 3 each in triplicates). *B*, $FeSO_4$ caused a time-dependent and dose-dependent increase in *Per1* mRNA expression and decrease in *Per2* mRNA expression in livers of mice. Mice were intravenously injected with iron $FeSO_4$ in doses of 10, 20, and 40 μmol/kg bw for 16 h and were injected with 40 μmol/kg of $FeSO_4$ and sacrificed after 4, 8, and 16 h. Mice were sacrificed at ZT1 to analyze *Per1* mRNA expression and ZT13 to analyze *Per2* mRNA expression (n = 4). *C*, quantification of intracellular ROS levels in RBCs incubated in PBS with or without 20 μM $FeSO_4$ at 37 °C for 20 min (n = 3 each in triplicates). *D*, fluorescence microscopic analysis of ROS generation in RBCs incubated in

regulates circadian cycle *via* functioning as a cofactor of clock genes, including NPAS2, PER2, CLOCK, and REV-ERB α/β (53, 54). The circadian regulation of iron in age may not act through heme because hepatic heme level is not increased during aging (55). In the present study, we discovered the consistent changes of six clock genes in the liver of old and iron-overload mice. All these suggest that iron accumulation may be a driven factor in inducing circadian and sleep disturbances in the old.

Monthly iron loss by menstruation may delay iron accumulation in premenopausal females. Body iron stores increase with age in males, whereas body iron stores in females increase substantially after menopause, and the average body iron stores in males are significantly higher than that in females (56). The incidence of heart disease in men and postmenopausal women is greater compared with that in premenopausal women, which has been attributed to higher iron stores (57). Phlebotomy is one of the most widely used methods to decrease systemic iron levels (58). Therefore, blood donation or phlebotomy is a feasible strategy to remove excess iron. Some studies have demonstrated that lowering iron stores by blood donation or phlebotomy can improve insulin resistance (59, 60). Blood donation has been associated with health benefits, including decreased mortality, decreased risk of myocardial infarction, and improved physical health in old donors and mental health in young donors (61–64). Blood donation is reported to decrease oxidative stress and increase the activity of antioxidant enzymes (65, 66). Thus, it is pretty easy to understand that phlebotomy declines iron accumulation, reversing metabolic patterns and restoring the circadian rhythms in old mice.

We have known that histone methylation is involved in the regulation of gene expression. H3K4me3 and H3K9me2 are common marks for transcriptional activating and silencing, respectively (67). In iron-overload or old mice, AMP resulted in elevating intracellular adenosine levels and reducing SAM/SAH ratio. Decreased SAM/SAH ratio led to decrease in global levels of histone H3K4me3 and H3K9me2. The decreased H3K4me3 and H3K9me2 have been found in old flies (68, 69). Intriguingly, AMP induced specific reduction of H3K9me2 levels in *Per1* promoters and H3K4me3 levels in *Per2* promoters. The plasma AMP can be converted to adenosine by CD73 (70), which is reported to be elevated in the aged heart and brain (71, 72). The release of adenosine is also significantly increased in aging human fibroblasts (73). Aging is associated with persistent inflammatory status (74, 75), ATP release increases under inflammatory conditions (76), which may contribute to the increment in AMP and adenosine levels during aging process. Then we proposed a hypothesis that the specific regulation of AMP is because of different nucleosome structures in *Per1* and *Per2* promoters. As shown in Figure 7*K*, DNA in promoters wraps around a histone octamer in a left-handed way, forming a stable nucleosome structure. In the *Per1* promoter, the H3K4 lysine residues are proposed to locate inside the nucleosome, whereas the H3K9 lysine residues are extended outward. On the contrary, the H3K9 lysine residues are proposed to locate inside the *Per2* promoter, whereas the H3K4 lysine residues are splayed outward. The methylation of exposed lysine residues is able to be affected by cellular methylation potential, but the lysine residues located inside the nucleosomes can hardly be modified. Finally, iron is a hard metal used to make many types of cooking utensils, and almost all food and drinking items contain more or less amount of iron. For people after middle age, it is time to choose to reduce iron intake and reasonably donate their blood for their health.

Experimental procedures

Animals

Four-week-old and 60-week-old male C57BL/6 mice were purchased from the Laboratory Animal Center at Yangzhou University. All mice were housed in a standard animal facility under a 12 h/12 h light/dark cycle with free access to food and water. Mice were allowed to acclimate for at least 1 week after arrival before experimentation. All procedures were approved by the Animal Care and Use Committee at Nanjing University of Science and Technology (ACUC-NUST-20180313).

Establishment of the mouse models

Iron-overload mice models were established by intraperitoneal injection of iron dextran or feeding with a high-iron diet. Iron dextran (5 mg/mouse/day) in 100 μl PBS was injected intraperitoneally twice a week for 3 weeks to induce iron overload, as previously described (77). Alternatively, mice were fed a 2.5% carbonyl iron-supplemented diet for 2 weeks as previously described (78). About 2.5% carbonyl iron–supplemented diet was prepared as described previously (79). Briefly, carbonyl iron was mixed with powdered standard diet (Jiangsu Xietong Pharmaceutical Bio-engineering Co, Ltd) in a ratio of 2.5% (w/w) and then made into pellets and dried. For phlebotomy, 64-week-old male C57BL/6 mice were bled by 100 and 200 μl of blood *via* cheek puncture. Mice were sacrificed 2 weeks after phlebotomy.

PBS with or without 20 μM $FeSO_4$ at 37 °C for 20 min (n = 3 each in triplicates; the scale bars represent 20 μm). *E*, quantification of ROS levels in lysates of RBCs incubated in PBS with or without 20 μM $FeSO_4$ at 37 °C for 20 min by a fluorescence spectrophotometer (n = 5 each in triplicates). *F*, $FeSO_4$ induced dose-dependent hemolysis in whole blood. Whole blood was incubated with or without $FeSO_4$ (10, 20, or 50 μM) at 37 °C for 20 min, and the absorbance of the supernatant was measured at 540 nm. Hemolysis is expressed as in absorbance values at 540 nm (n = 3 each in triplicates). *G*, representative HPLC profiles of nucleotides from the extracts of plasma from mice intravenously injected with $FeSO_4$ in doses of 20 or 40 μmol/kg bw. Mice were sacrificed 2 h after $FeSO_4$ administration to collect blood samples (n = 5). *H*, *left*, quantification of plasma AMP after $FeSO_4$ treatment (n = 5). *Right*, HPLC analysis of plasma AMP in young (8 weeks old) and old (64 weeks old) mice with or without 0.2 ml phlebotomy. OLD, old mice group; OLD + PH, old mice with 0.2 ml phlebotomy group; YNG, young mice group. Mice were sacrificed 2 weeks after blood donation. *Asterisk* indicates significant difference compared with the YNG group. *$p < 0.05$; **$p < 0.01$; # indicates significant difference compared with the OLD group. #$p < 0.05$; ##$p < 0.01$ (n = 6). *I*, AMP caused increased *Per1* mRNA expression and decreased *Per2* mRNA expression. Mice were i.p. injected with AMP (0.5 μmol/g bw) at ZT1 and ZT13 to analyze *Per1* and *Per2* mRNA expression, respectively. Mice were sacrificed 1 h after AMP administration (n = 4). All data are expressed as mean ± SD, *$p < 0.05$, **$p < 0.01$. bw, body weight; RBC, red blood cell; ROS, reactive oxygen species

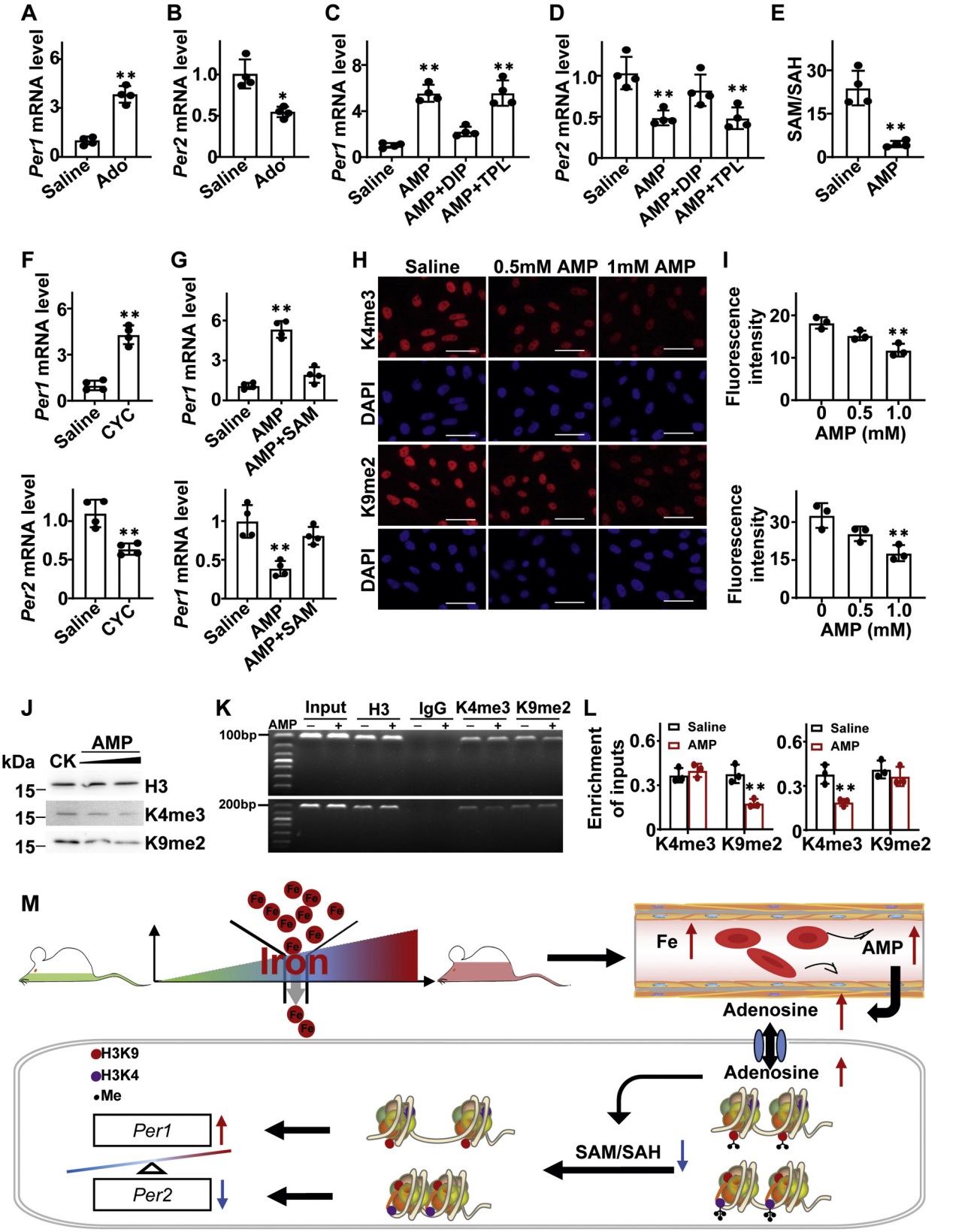

Figure 7. AMP reciprocally regulates *Per1* and *Per2* transcription. *A*, quantitative RT–PCR analysis of *Per1* mRNA in mice treated with adenosine. Mice were i.p. injected with adenosine (Ado, 0.2 μmol/g bw) at ZT1 to analyze *Per1* mRNA expression. Saline served as the control. Mice were sacrificed 1 h after adenosine administration (n = 4). *B*, quantitative RT–PCR analysis of *Per2* mRNA in mice treated with adenosine. Mice were i.p. injected with adenosine (Ado, 0.2 μmol/g bw) at ZT13 to analyze *Per2* mRNA expression. Saline served as the control. Mice were sacrificed 1 h after adenosine administration (n = 4). *C*, quantitative RT–PCR analysis of *Per1* mRNA in NIH3T3 cells treated with theophylline (TPL, 100 μM), dipyridamole (DIP, 0.1 μM), plus AMP (0.5 mM) for 24 h, respectively (n = 4 each in triplicates). *D*, quantitative RT–PCR analysis of *Per2* mRNA in NIH3T3 cells treated with TPL (100 μM), DIP (0.1 μM), plus AMP

Iron studies for serum and tissues

Serum iron, Tf saturation, total iron-binding capacity, and unbound iron-binding capacity were determined using commercially available assay kits (Nanjing Jincheng Bioengineering Institute). Tissue iron levels were determined as previously described (80). Tissue samples were dried at 106 °C overnight to constant mass and weighed again. Dried samples were ashed in the oven at 500 °C for 17 h and then fully solubilized in 6 M HCl. And the final solution was adjusted with demineralized water to a final HCl concentration of 1.2 M. Iron concentration of the samples was determined by flame atomic absorption spectrometry (Varian SpectrAA 250 Plus; Varian).

Treatment of AMP, adenosine, and $FeSO_4$

AMP and adenosine (Sigma) were dissolved in saline and administered to mice by intraperitoneal injection in a dose of 0.5 μmol/g and 0.2 μmol/g body weight (bw), respectively. To investigate dose-dependent and time-dependent changes of *Per1* and *Per2* mRNA expression after iron treatment, mice were injected intravenously with $FeSO_4$ in the doses of 10, 20, and 40 μmol/kg bw for 16 h and were injected with 40 μmol/kg bw of $FeOS_4$ and sacrificed at 4, 8, and 16 h. To investigate the effects of iron on plasma nucleotides, mice were intravenously injected with $FeSO_4$ in doses of 20 and 40 μmol/kg bw. Mice were sacrificed 2 h after $FeSO_4$ administration. Saline served as a control for all experiments described previously.

HPLC analysis for nucleotides

Blood samples (heparin sodium anticoagulation) were immediately centrifuged at 5000*g* for 5 min at 4 °C. Nucleotides were extracted from the plasma using 0.4 N perchloric acid solution and analyzed by HPLC (81). Extracts were separated and quantified using reverse-phase HPLC (Waters 1525 System; Millipore) on a reversed-phase C18 column as described previously (81–83). SAM and SAH were extracted from cold PBS-washed cell monolayers or frozen liver samples using 0.4 N perchloric acid (84). SAM and SAH were measured by a reverse-phase HPLC according to the procedure previously described (85). Standards were used to identify the peaks and make the calibration curves. Quantification was based on the peak areas. SAM was from Solarbio. AMP and SAH were from Sigma. The HPLC chromatogram of AMP standard detected at 260 nm with maximum absorption wavelength at 257.9 nm is provided in Fig. S7.

Determination of intracellular ROS contents in RBCs and hemolysis assay

RBCs were purified as previously described (86). The purified RBCs (~10^6 RBCs/ml) were incubated with 2'-7'dichlorofluorescin diacetate (0.4 mM final concentration) at 37 °C for 15 min. After being washed twice, the RBCs were then incubated in PBS at 37 °C with or without $FeSO_4$ (20 μM) for 20 min. After incubation, the intracellular ROS contents in RBCs were quantified by flow cytometry as described previously (87–89). Also, the ROS levels were visualized by fluorescence microscopy, and the ROS levels in RBC lysates were quantified by a fluorescent spectrophotometer. Hemolysis in whole blood was evaluated spectrophotometrically at 540 nm of the supernatant after a 20 min incubation with or without $FeSO_4$ (20 μM) for 20 min at 37 °C, as described previously (90).

Cell culture

NIH3T3 cells were grown in Dulbecco's modified Eagle's medium (DMEM) supplemented with 10% fetal bovine serum (FBS; Gibco) and penicillin/streptomycin (10 μl/ml of medium; Gibco) at 37 °C in 5% (v/v) CO_2. Serum shock was performed for synchronization as previously described (91). Briefly, after cells were grown to confluency in 6-well plates, the medium was exchanged by 50% horse serum (Gibco) in DMEM; after 2 h (t = 0), the medium was removed and replaced with fresh 0.5% FBS-containing medium. To investigate the effects mediated by adenosine, cells were then treated with various concentrations of the compounds to be analyzed for 24 h: vehicle, AMP (0.5 mM) alone, AMP (0.5 mM) plus dipyridamole (0.1 μM), or theophylline (100 μM). To analyze the effects of cellular methylation potential, cells were treated with 20 mM cycloleucine for 24 h to inhibit methylation, and cells were also treated with AMP (0.5 mM) for 24 h with or without 2 mM SAM after synchronization. At indicated time, cells were harvested for total RNA extraction.

(0.5 mM) for 24 h, respectively (n = 4 each in triplicates). *E*, HPLC analysis of SAM and SAH in NIH3T3 cells treated with AMP (0.5 mM) for 24 h (n = 4 each in triplicates). *F*, quantitative RT–PCR analysis of *Per1* and *Per2* mRNA in NIH3T3 cells treated with cycloleucine (CYC, 20 mM) for 24 h, respectively (n = 4 each in triplicates). *G*, quantitative RT–PCR analysis of *Per1* and *Per2* mRNA in NIH3T3 cells treated with SAM (2 mM) plus AMP (0.5 mM) for 24 h (n = 4 each in triplicates). *H*, representative fluorescence images showing that AMP decreased global H3K4me3 and H3K9me2 levels in NIH3T3 cells. The H3K4me3 and H3K9me2 were visualized by immunofluorescence with specific antibodies (*red*). Nuclei were stained with DAPI. NIH3T3 cells were treated with 0.5 mM or 1 mM AMP for 24 h. Saline served as the control (n = 3 each in triplicates; the scale bars represent 20 μm). *I*, immunofluorescence signal quantification of H3K4me3 (*top*) and H3K9me2 (*bottom*) in *H* (n = 3 each in triplicates). *J*, Western blot analysis of H3K4me3 and H3K9me2 levels in NIH3T3 cells treated with AMP. NIH3T3 cells were treated with 0.5 mM or 1 mM AMP for 24 h. Saline served as the control (n = 3 each in triplicates). *K*, ChIP analysis using the antibody against trimethyl-Histone H3 Lys4 (H3K4me3) or dimethyl-Histone H3 Lys9 (H3K9me2), followed by PCR with primers amplifying the *Per1* and *Per2*. Input, IgG, and H3 serve as controls. The representative images showed that the level of H3K9me2 at the *Per1* promoter region and the level of H3K4me3 at the *Per2* promoter region were decreased after AMP (0.5 mM) treatment. Mice were sacrificed 1 h after AMP administration at ZT13 (n = 3 each in triplicates). *L*, quantification of the enrichment in H3K4me3 and H3K9me2 with quantitative RT–PCR analysis. Input-DNA and ChIP-DNA samples were quantified using primers for the promoters of the *Per1* and *Per2* genes (n = 3 each in triplicates). *M*, schematic representation of the proposed mechanism of how accumulating iron regulates *Per1* and *Per2* transcription during aging. Elevated serum iron induces AMP release from RBCs, and increased AMP is converted to adenosine by CD73. Adenosine is transported into hepatocyte and reduces SAM to SAH ratio, thus decreasing the global histone methylation. A hypothesis showing the H3K9 residues are exposed outside the nucleosome with H3K4 residues buried inside in the *Per1* promoter; and the H3K4 residues are exposed outside the nucleosome with H3K9 residues buried inside in the *Per2* promoter. All data are expressed as the means ± SD, $*p < 0.05$, $**p < 0.01$. bw, body weight; ChIP, chromatin immunoprecipitation; DAPI, 4′,6-diamidino-2-phenylindole; IgG, immunoglobulin G; RBC, red blood cell.

Real-time luciferase reporter assays

Luciferase reporter assays were conducted as previously described (92). The *Per1*-dLuc and *Per2*-dLuc reporter plasmids were generated by cloning the mouse *Per1*-promoter (−1803 to + 40) or mouse *Per2* promoter (−1670 to +53) into pGL3-dLuc, respectively (93). Then 2 μg of each reporter plasmid was transfected into NIH3T3 cells (35 mm dish) using HilyMax (DOJINDO Laboratories), respectively. The cells were stimulated with 100 nm dexamethasone (Sigma–Aldrich) for 2 h in serum-free DMEM, and then the medium was replaced with fresh DMEM containing 100 μM luciferin (Wako Pure Chemical Industries), 25 mm Hepes (pH 7.2), 10% FBS, and with or without 10 or 20 μM $FeSO_4$. Bioluminescence was recorded and integrated for 1 min at intervals of 10 min using the LumiCycle (Actimetrics). The cells were cultured in a luminometer for 3 days to evaluate bioluminescence.

RNA extraction and quantitative real-time PCR

Total RNA was extracted from livers and cells with Karrol reagent (Karroten) according to the manufacturer's instructions. RT reaction was carried out by reverse transcript kit (Karroten) according to the manufacturer's protocol. Real-time PCR was performed with the SYBR Green PCR Kit (Karroten) using an ABI 7300plus Detection System (Applied Biosystems). The results were normalized to β-actin. The sequences of all primers are listed in Table S5.

RNA-Seq and analysis

Purified total RNA from the liver was used for RNA-Seq preparation. The complementary DNA library construction and sequencing were performed by Beijing Genomics Institute using a BGISEQ-500 platform. High-quality reads were aligned to the mouse reference genome using Bowtie2 (http://bowtie-bio.sourceforge.net/bowtie2/index.shtml). The expression levels for each gene were calculated and normalized to fragments per kilobase of exon model per million mapped reads.

Histologic examination

A histologic examination was performed according to the method described previously (94, 95). Briefly, liver tissue was fixed with 4% paraformaldehyde in PBS overnight. The tissues were then transferred to 70% ethanol and embedded in paraffin. Samples were cut into 5 μm sections and stained with H&E. Ferric iron was visualized with DAB-enhanced Prussian Blue staining. Briefly, deparaffinized and rehydrated tissue sections (5 μm) were incubated at 37 °C for 1 h in 7% potassium ferrocyanide with aqueous hydrochloric acid (3%) and subsequently incubated in 0.75 mg/ml DAB and 0.015% H_2O_2 for 5 to 10 min.

^{1}H NMR sample preparation and NMR spectroscopy

Metabolites were extracted from livers in YNG (young group), OLD (old group), and HI (iron-overload group) following previously reported protocols (96). Briefly, approximately 200 mg of liver samples were homogenized in 2 ml ice-cold acetonitrile/water (1:1 v/v) buffer. After centrifugation (12,000*g*, 4 °C) for 10 min, the supernatant was collected into glass vials. Then most acetonitrile in the supernatant was removed using a gentle stream of nitrogen. Next, the aqueous residues were freeze-dried and stored at −80 °C until further analysis. For NMR analysis, the lyophilized samples were reconstituted in 600 μl heavy water phosphate buffer (0.2 M, pH 7.4) containing 0.05% trimethylsilylpropanoic acid as a chemical shift reference. NMR spectra were recorded on a Bruker AVANCE III 500 MHz NMR spectrometer at 298 K.

Spectra processing and data analysis

The ^{1}H NMR spectra were manually phased, baseline corrected, and referenced to trimethylsilylpropanoic acid using Bruker TOPSPIN 3.0 software. And MestReC (version 3.7.4: Mestrelab Research SL) was used to export ^{1}H NMR spectra to ASCII files before importing them into R software (http://cran.r-project.org/) to analyze data. After peak alignment, the water signals and affected regions from 4.7 to 5.1 ppm were discarded. The remaining spectra were mean-centered and Pareto-scaled to facilitate multivariate analysis. A supervised OPLS-DA was conducted to filter irrelevant systematic signals and explore the major features between two groups. The score plots showed the discrimination of categories, and loading plots indicated significantly altered metabolites that contributed to the discrimination. The OPLS-DA models were validated by repeated crossvalidations. Identification of metabolites was performed using Chenomx NMR Suite software (version 7.7; Chenomx) and published articles. Also, unsupervised principal component analysis was carried out to compare the differences among all three groups.

ChIP assays

ChIP assays were conducted as described previously (97, 98). Cross-linked chromatin was immunoprecipitated with 5 μg of anti-Histone H3 (Abcam; catalog no.: ab1791), anti–trimethyl-Histone H3 Lys4 (Abcam; catalog no.: ab8580), anti–dimethyl-Histone H3 Lys9 (Abcam; catalog no.: ab1220), respectively, or negative control rabbit immunoglobulin G. Immunoprecipitated DNA was then purified and used as a template for PCR analysis. The primer sequences used for PCR are listed in Table S6.

Immunofluorescence analysis

Immunofluorescence was performed as described previously (99). Briefly, NIH3T3 cells were washed three times with cold PBS, fixed with 4% paraformaldehyde for 15 min, and permeabilized with 0.25% Triton X-100 (Sigma) for 10 min. Fixed cells were incubated with primary antibodies anti–trimethyl-Histone H3 Lys4 (Abcam; catalog no.: ab8580), anti–dimethyl-Histone H3 Lys9 (Abcam; catalog no.: ab1220), and Alexa Fluor 568–conjugated secondary antibodies step by step. Nuclei were stained with 4′,6-diamidino-2-phenylindole. Then the samples were imaged with fluorescence microscopy (Eclipse Ti2; Nikon) and processed using NIS-Element Version 5.02 software (Nikon, Melville, NY).

Statistical analysis

Data without indications were presented as means ± SD. Independent replicates for each data point (n) are identified in figure legends. Data graphics and statistical analysis were performed using GraphPad Prism 8 software (GraphPad Software, Inc). Statistical difference between two groups was determined by Student's *t* test, and comparisons among groups were performed using ANOVA. A *p* value of less than 0.05 was regarded as statistically significant.

Data availability

All data of this study are available in this article and the supporting information. All source data generated for this study and relevant information are available from the corresponding author.

Supporting information—This article contains supporting information.

Acknowledgments—This research work was supported by the National Natural Science Foundation of China fund (grant nos.: 31861163004 and 31871178) and the Fundamental Research Funds for the Central Universities (grant nos.: 30920031102).

Author contributions—J. Z. conceptualization; Y. Z. and T. C. methodology; Y. Z. software; Z. D., Y. Z., and W. G. validation; J. L. and T. C. formal analysis; Y. Z., Z. D., and J. L. investigation; Z. D. and Y. Z. resources; J. L. writing–original draft; J. Z., J. L., and Z. D. writing–review & editing; J. L., Y. Z., and W. G. visualization; J. Z. supervision; J. Z. project administration; J. Z. funding acquisition.

Conflict of interest—The authors declare that they have no conflicts of interest with the contents of this article.

Abbreviations—The abbreviations used are: bw, body weight; CAT, catalase; ChIP, chromatin immunoprecipitation; DAB, diaminobenzidine; DEG, differentially expressed gene; DMEM, Dulbecco's modified Eagle's medium; FBS, fetal bovine serum; KEGG, Kyoto Encyclopedia of Genes and Genomes; OPLS-DA, orthogonal partial least squares discriminant analysis; RBC, red blood cell; ROS, reactive oxygen species; Tf, transferrin.

References

1. Madeddu, C., Gramignano, G., Astara, G., Demontis, R., Sanna, E., Atzeni, V., and Macciò, A. (2018) Pathogenesis and treatment options of cancer related anemia: Perspective for a targeted mechanism-based approach. *Front. Physiol.* **9**, 1294
2. Stoltzfus, R. J. (2003) Iron deficiency: Global prevalence and consequences. *Food Nutr. Bull.* **24**, S99–S103
3. Ayala, A., Muñoz, M. F., and Argüelles, S. (2014) Lipid peroxidation: Production, metabolism, and signaling mechanisms of malondialdehyde and 4-hydroxy-2-nonenal. *Oxidative Med. Cell. Longev.* **2014**, 360438
4. Mehta, K. J., Farnaud, S. J., and Sharp, P. A. (2019) Iron and liver fibrosis: Mechanistic and clinical aspects. *World J. Gastroenterol.* **25**, 521
5. Torti, S. V., and Torti, F. M. (2013) Iron and cancer: More ore to be mined. *Nat. Rev. Cancer* **13**, 342–355
6. Jung, M., Weigert, A., Mertens, C., Rehwald, C., and Brüne, B. (2017) Iron handling in tumor-associated macrophages—is there a new role for lipocalin-2? *Front. Immunol.* **8**, 1171
7. Boult, J., Roberts, K., Brookes, M. J., Hughes, S., Bury, J. P., Cross, S. S., Anderson, G. J., Spychal, R., Iqbal, T., and Tselepis, C. (2008) Overexpression of cellular iron import proteins is associated with malignant progression of esophageal adenocarcinoma. *Clin. Cancer Res.* **14**, 379–387
8. Schoenfeld, J. D., Sibenaller, Z. A., Mapuskar, K. A., Wagner, B. A., Cramer-Morales, K. L., Furqan, M., Sandhu, S., Carlisle, T. L., Smith, M. C., and Hejleh, T. A. (2017) O2·– and H2O2-mediated disruption of Fe metabolism causes the differential susceptibility of NSCLC and GBM cancer cells to pharmacological ascorbate. *Cancer cell* **31**, 487–500.e488
9. Mercadante, C. J., Prajapati, M., Parmar, J. H., Conboy, H. L., Dash, M. E., Pettiglio, M. A., Herrera, C., Bu, J. T., Stopa, E. G., and Mendes, P. (2019) Gastrointestinal iron excretion and reversal of iron excess in a mouse model of inherited iron excess. *Haematologica* **104**, 678
10. Prajapati, M., Conboy, H. L., Hojyo, S., Fukada, T., Budnik, B., and Bartnikas, T. B. (2021) Biliary excretion of excess iron in mice requires hepatocyte iron import by Slc39a14. *J. Biol. Chem.* **297**, 100835
11. Andrews, N. C. (1999) Disorders of iron metabolism. *New Engl. J. Med.* **341**, 1986–1995
12. McKie, A. T., Barrow, D., Latunde-Dada, G. O., Rolfs, A., Sager, G., Mudaly, E., Mudaly, M., Richardson, C., Barlow, D., and Bomford, A. (2001) An iron-regulated ferric reductase associated with the absorption of dietary iron. *Science* **291**, 1755–1759
13. Gunshin, H., Mackenzie, B., Berger, U. V., Gunshin, Y., Romero, M. F., Boron, W. F., Nussberger, S., Gollan, J. L., and Hediger, M. A. (1997) Cloning and characterization of a mammalian proton-coupled metal-ion transporter. *Nature* **388**, 482–488
14. Korolnek, T., and Hamza, I. (2014) Like iron in the blood of the people: The requirement for heme trafficking in iron metabolism. *Front. Pharmacol.* **5**, 126
15. Ganz, T. (2013) Systemic iron homeostasis. *Physiol. Rev.* **93**, 1721–1741
16. Xu, J., Jia, Z., Knutson, M. D., and Leeuwenburgh, C. (2012) Impaired iron status in aging research. *Int. J. Mol. Sci.* **13**, 2368–2386
17. Massie, H. R., Aiello, V. R., and Banziger, V. (1983) Iron accumulation and lipid peroxidation in aging C57BL/6J mice. *Exp. Gerontol.* **18**, 277–285
18. Sohal, R. S., Wennberg-Kirch, E., Jaiswal, K., Kwong, L. K., and Forster, M. J. (1999) Effect of age and caloric restriction on bleomycin-chelatable and nonheme iron in different tissues of C57BL/6 mice. *Free Radic. Biol. Med.* **27**, 287–293
19. Cook, C. I., and Yu, B. P. (1998) Iron accumulation in aging: Modulation by dietary restriction. *Mech. Ageing Dev.* **102**, 1–13
20. Xu, J., Knutson, M. D., Carter, C. S., and Leeuwenburgh, C. (2008) Iron accumulation with age, oxidative stress and functional decline. *PLoS one* **3**, e2865
21. Berdoukas, V., Coates, T. D., and Cabantchik, Z. I. (2015) Iron and oxidative stress in cardiomyopathy in thalassemia. *Free Radic. Biol. Med.* **88**, 3–9
22. Kalpravidh, R. W., Tangjaidee, T., Hatairaktham, S., Charoensakdi, R., Panichkul, N., Siritanaratkul, N., and Fucharoen, S. (2013) Glutathione redox system in β-Thalassemia/Hb E patients. *Sci. World J.* **2013**, 543973
23. Lass, A., Sohal, B. H., Weindruch, R., Forster, M. J., and Sohal, R. S. (1998) Caloric restriction prevents age-associated accrual of oxidative damage to mouse skeletal muscle mitochondria. *Free Radic. Biol. Med.* **25**, 1089–1097
24. Silva, R. H., Abílio, V. C., Takatsu, A., Kameda, S. R., Grassl, C., Chehin, A. B., Medrano, W. A., Calzavara, M. B., Registro, S., and Andersen, M. L. (2004) Role of hippocampal oxidative stress in memory deficits induced by sleep deprivation in mice. *Neuropharmacology* **46**, 895–903
25. Schmucker, D. L. (2005) Age-related changes in liver structure and function: Implications for disease? *Exp. Gerontol.* **40**, 650–659
26. Bliwise, D. L. (1993) Sleep in normal aging and dementia. *Sleep* **16**, 40–81
27. Turek, F. W., Penev, P., Zhang, Y., Van Reeth, O., and Zee, P. (1995) Effects of age on the circadian system. *Neurosci. Biobehavioral. Rev.* **19**, 53–58
28. Van Someren, E. (2000) Circadian and sleep disturbances in the elderly. *Exp. Gerontol.* **35**, 1229–1237
29. Tarasiuk, A., Ali, A.-H., Moser, A., Freidman, B., Tal, A., and Kapelushnik, J. (2003) Sleep disruption and objective sleepiness in children

with β-thalassemia and congenital dyserythropoietic anemia. *Arch. Pediatr. Adolesc. Med.* **157**, 463–468
30. Wallen, G. R., Minniti, C. P., Krumlauf, M., Eckes, E., Allen, D., Oguhebe, A., Seamon, C., Darbari, D. S., Hildesheim, M., and Yang, L. (2014) Sleep disturbance, depression and pain in adults with sickle cell disease. *BMC Psychiatry* **14**, 1–8
31. Castro-Caraballo, F., Suarez-Roca, H., Estevez, J., and Bonilla, E. (1992) Spontaneous motor activity in mice overloaded with iron-dextran. *Invest. Clin.* **33**, 121–134
32. Beard, J. L. (2001) Iron biology in immune function, muscle metabolism and neuronal functioning. *J. Nutr.* **131**, 568S–580S
33. Prá, D., Rech Franke, S. I., Pegas Henriques, J. A., and Fenech, M. (2009) A possible link between iron deficiency and gastrointestinal carcinogenesis. *Nutr. Cancer* **61**, 415–426
34. Ellervik, C., Andersen, H. U., Tybjærg-Hansen, A., Frandsen, M., Birgens, H., Nordestgaard, B. G., and Mandrup-Poulsen, T. (2013) Total mortality by elevated transferrin saturation in patients with diabetes. *Diabetes Care* **36**, 2646–2654
35. Hörl, W. H., and Schmidt, A. (2014) Low hepcidin triggers hepatic iron accumulation in patients with hepatitis C. *Nephrol. Dial. Transplant.* **29**, 1141–1144
36. Kijima, H., Sawada, T., Tomosugi, N., and Kubota, K. (2008) Expression of hepcidin mRNA is uniformly suppressed in hepatocellular carcinoma. *BMC Cancer* **8**, 1–8
37. Andrews, N. C. (2008) Forging a field: The golden age of iron biology. *Blood J. Am. Soc. Hematol.* **112**, 219–230
38. Krebs, N. F. (2000) Dietary zinc and iron sources, physical growth and cognitive development of breastfed infants. *J. Nutr.* **130**, 358S–360S
39. Mpoya, A., Kiguli, S., Olupot-Olupot, P., Opoka, R. O., Engoru, C., Mallewa, M., Chimalizeni, Y., Kennedy, N., Kyeyune, D., and Wabwire, B. (2015) Transfusion and treatment of severe anaemia in African children (TRACT): A study protocol for a randomised controlled trial. *Trials* **16**, 1–15
40. Camaschella, C. (2005) Understanding iron homeostasis through genetic analysis of hemochromatosis and related disorders. *Blood* **106**, 3710–3717
41. Knutson, M. D., Walter, P. B., Ames, B. N., and Viteri, F. E. (2000) Both iron deficiency and daily iron supplements increase lipid peroxidation in rats. *J. Nutr.* **130**, 621–628
42. Huang, D., Wei, W., Xie, F., Zhu, X., Zheng, L., and Lv, Z. (2018) Steroidogenesis decline accompanied with reduced antioxidation and endoplasmic reticulum stress in mice testes during ageing. *Andrologia* **50**, e12816
43. Voss, P., and Siems, W. (2006) Clinical oxidation parameters of aging. *Free Radic. Res.* **40**, 1339–1349
44. Praharaj, S. K., Gupta, R., and Gaur, N. (2018) Clinical practice guideline on management of sleep disorders in the elderly. *Indian J. Psychiatry* **60**, S383
45. Mohawk, J. A., Green, C. B., and Takahashi, J. S. (2012) Central and peripheral circadian clocks in mammals. *Annu. Rev. Neurosci.* **35**, 445–462
46. Hofman, M. A., and Swaab, D. F. (2006) Living by the clock: The circadian pacemaker in older people. *Ageing Res. Rev.* **5**, 33–51
47. Huang, Y.-L., Liu, R.-Y., Wang, Q.-S., Van Someren, E. J., Xu, H., and Zhou, J.-N. (2002) Age-associated difference in circadian sleep–wake and rest–activity rhythms. *Physiol. Behav.* **76**, 597–603
48. Kondratova, A. A., and Kondratov, R. V. (2012) The circadian clock and pathology of the ageing brain. *Nat. Rev. Neurosci.* **13**, 325–335
49. Crowley, K. (2011) Sleep and sleep disorders in older adults. *Neuropsychol. Rev.* **21**, 41–53
50. Ancoli-Israel, S., and Ayalon, L. (2009) Diagnosis and treatment of sleep disorders in older adults. *Focus* **7**, 98–105
51. Simcox, J. A., Mitchell, T. C., Gao, Y., Just, S. F., Cooksey, R., Cox, J., Ajioka, R., Jones, D., Lee, S.-h., and King, D. (2015) Dietary iron controls circadian hepatic glucose metabolism through heme synthesis. *Diabetes* **64**, 1108–1119
52. Kaasik, K., and Lee, C. C. (2004) Reciprocal regulation of haem biosynthesis and the circadian clock in mammals. *Nature* **430**, 467–471
53. Raghuram, S., Stayrook, K. R., Huang, P., Rogers, P. M., Nosie, A. K., McClure, D. B., Burris, L. L., Khorasanizadeh, S., Burris, T. P., and Rastinejad, F. (2007) Identification of heme as the ligand for the orphan nuclear receptors REV-ERBα and REV-ERBβ. *Nat. Struct. Mol. Biol.* **14**, 1207–1213
54. Kitanishi, K., Igarashi, J., Hayasaka, K., Hikage, N., Saiful, I., Yamauchi, S., Uchida, T., Ishimori, K., and Shimizu, T. (2008) Heme-binding characteristics of the isolated PAS-A domain of mouse Per2, a transcriptional regulatory factor associated with circadian rhythms. *Biochemistry* **47**, 6157–6168
55. Abraham, N. G., Levere, R. D., and Freedman, M. L. (1985) Effect of age on rat liver heme and drug metabolism. *Exp. Gerontol.* **20**, 277–284
56. Toyokuni, S. (2011) Iron as a target of chemoprevention for longevity in humans. *Free Radic. Res.* **45**, 906–917
57. Jian, J., Pelle, E., and Huang, X. (2009) *Iron and Menopause: Does Increased Iron Affect the Health of Postmenopausal Women?*, Mary Ann Liebert, Inc, New Rochelle, NY
58. Schwartz, A. J., Das, N. K., Ramakrishnan, S. K., Jain, C., Jurkovic, M. T., Wu, J., Nemeth, E., Lakhal-Littleton, S., Colacino, J. A., and Shah, Y. M. (2019) Hepatic hepcidin/intestinal HIF-2α axis maintains iron absorption during iron deficiency and overload. *J. Clin. Invest.* **129**, 336–348
59. Equitani, F., Fernandez-Real, J. M., Menichella, G., Koch, M., Calvani, M., Nobili, V., Mingrone, G., and Manco, M. (2008) Bloodletting ameliorates insulin sensitivity and secretion in parallel to reducing liver iron in carriers of HFE gene mutations. *Diabetes Care* **31**, 3–8
60. Fernández-Real, J. M., Peñarroja, G., Castro, A., García-Bragado, F., López-Bermejo, A., and Ricart, W. (2002) Blood letting in high-ferritin type 2 diabetes: Effects on vascular reactivity. *Diabetes care* **25**, 2249–2255
61. Ullum, H., Rostgaard, K., Kamper-Jørgensen, M., Reilly, M., Melbye, M., Nyrén, O., Norda, R., Edgren, G., and Hjalgrim, H. (2015) Blood donation and blood donor mortality after adjustment for a healthy donor effect. *Transfusion* **55**, 2479–2485
62. Vahidnia, F., Hirschler, N. V., Agapova, M., Chinn, A., Busch, M. P., and Custer, B. (2013) Cancer incidence and mortality in a cohort of US blood donors: A 20-year study. *J. Cancer Epidemiol.* **2013**, 814842
63. Rigas, A., Skytthe, A., Erikstrup, C., Rostgaard, K., Petersen, M., Hjalgrim, H., Ullum, H., Kyvik, K., and Pedersen, O. (2019) The healthy donor effect impacts self-reported physical and mental health–results from the Danish Blood Donor Study (DBDS). *Transfus. Med.* **29**, 65–69
64. Salonen, J. T., Tuomainen, T.-P., Salonen, R., Lakka, T. A., and Nyyssonen, K. (1998) Donation of blood is associated with reduced risk of myocardial infarction: The kuopio ischaemic heart disease risk factor study. *Am. J. Epidemiol.* **148**, 445–451
65. Yunce, M., Erdamar, H., Bayram, N. A., and Gok, S. (2016) One more health benefit of blood donation: Reduces acute-phase reactants, oxidants and increases antioxidant capacity. *J. Basic Clin. Physiol. Pharmacol.* **27**, 653–657
66. van Jaarsveld, H., and Pool, G. F. (2002) Beneficial effects of blood donation on high density lipoprotein concentration and the oxidative potential of low density lipoprotein. *Atherosclerosis* **161**, 395–402
67. Chen, Y. W., Kao, S. Y., Wang, H. J., and Yang, M. H. (2013) Histone modification patterns correlate with patient outcome in oral squamous cell carcinoma. *Cancer* **119**, 4259–4267
68. Wood, J. G., Hillenmeyer, S., Lawrence, C., Chang, C., Hosier, S., Lightfoot, W., Mukherjee, E., Jiang, N., Schorl, C., and Brodsky, A. S. (2010) Chromatin remodeling in the aging genome of Drosophila. *Aging cell* **9**, 971–978
69. Larson, K., Yan, S.-J., Tsurumi, A., Liu, J., Zhou, J., Gaur, K., Guo, D., Eickbush, T. H., and Li, W. X. (2012) Heterochromatin formation promotes longevity and represses ribosomal RNA synthesis. *PLoS Genet.* **8**, e1002473
70. Yegutkin, G. G. (2008) Nucleotide-and nucleoside-converting ectoenzymes: Important modulators of purinergic signalling cascade. *Biochim. Biophys. Acta (BBA)-Mol. Cell Res.* **1783**, 673–694
71. Lynch, G., and Gall, C. M. (2013) Mechanism based approaches for rescuing and enhancing cognition. *Front. Neurosci.* **7**, 143

72. Fenton, R. A., and Dobson, J. G., Jr. (2012) Reduced adenosine release from the aged mammalian heart. *J. Cell Physiol.* **227**, 3709–3714
73. Ethier, M. F., Hickler, R. B., and Dobson, J. G., Jr. (1989) Aging increases adenosine and inosine release by human fibroblast cultures. *Mech. Ageing Dev.* **50**, 159–168
74. Salminen, A., Huuskonen, J., Ojala, J., Kauppinen, A., Kaarniranta, K., and Suuronen, T. (2008) Activation of innate immunity system during aging: NF-kB signaling is the molecular culprit of inflamm-aging. *Ageing Res. Rev.* **7**, 83–105
75. Franceschi, C., Bonafè, M., Valensin, S., Olivieri, F., De Luca, M., Ottaviani, E., and De Benedictis, G. (2000) Inflamm-aging: An evolutionary perspective on immunosenescence. *Ann. New York Acad. Sci.* **908**, 244–254
76. Idzko, M., Ferrari, D., and Eltzschig, H. K. (2014) Nucleotide signalling during inflammation. *Nature* **509**, 310–317
77. Kawabata, H., Fleming, R. E., Gui, D., Moon, S. Y., Saitoh, T., O'Kelly, J., Umehara, Y., Wano, Y., Said, J. W., and Koeffler, H. P. (2005) Expression of hepcidin is down-regulated in TfR2 mutant mice manifesting a phenotype of hereditary hemochromatosis. *Blood* **105**, 376–381
78. Constante, M., Jiang, W., Wang, D., Raymond, V.-A., Bilodeau, M., and Santos, M. M. (2006) Distinct requirements for Hfe in basal and induced hepcidin levels in iron overload and inflammation. *Am. J. Physiol.-Gastrointestinal. Liver Physiol.* **291**, G229–G237
79. Arezzini, B., Lunghi, B., Lungarella, G., and Gardi, C. (2003) Iron overload enhances the development of experimental liver cirrhosis in mice. *Int. J. Biochem. Cel. Biol.* **35**, 486–495
80. Santos, M. M., de Sousa, M., Rademakers, L. H., Clevers, H., Marx, J., and Schilham, M. W. (2000) Iron overload and heart fibrosis in mice deficient for both β2-microglobulin and Rag1. *Am. J. Pathol.* **157**, 1883–1892
81. Knudsen, T., Winters, R., Otey, S., Blackburn, M., Airhart, M., Church, J., and Skalko, R. (1992) Effects of (R)-deoxycoformycin (pentostatin) on intrauterine nucleoside catabolism and embryo viability in the pregnant mouse. *Teratology* **45**, 91–103
82. Ramsey, K. M., Yoshino, J., Brace, C. S., Abrassart, D., Kobayashi, Y., Marcheva, B., Hong, H.-K., Chong, J. L., Buhr, E. D., and Lee, C. (2009) Circadian clock feedback cycle through NAMPT-mediated NAD+ biosynthesis. *Science* **324**, 651–654
83. Smolenski, R., Lachno, D., Ledingham, S., and Yacoub, M. (1990) Determination of sixteen nucleotides, nucleosides and bases using high-performance liquid chromatography and its application to the study of purine metabolism in hearts for transplantation. *J. Chromatogr. B: Biomed. Sci. Appl.* **527**, 414–420
84. Yang, X., Zhao, Y., Sun, Q., Yang, Y., Gao, Y., Ge, W., Liu, J., Xu, X., Weng, D., and Wang, S. (2019) Adenine nucleotide-mediated regulation of hepatic PTP1B activity in mouse models of type 2 diabetes. *Diabetologia* **62**, 2106–2117
85. Xia, L., Ma, S., Zhang, Y., Wang, T., Zhou, M., Wang, Z., and Zhang, J. (2015) Daily variation in global and local DNA methylation in mouse livers. *PLoS one* **10**, e0118101
86. Terman, D. S., Viglianti, B. L., Zennadi, R., Fels, D., Boruta, R. J., Yuan, H., Dreher, M. R., Grant, G., Rabbani, Z. N., and Moon, E. (2013) Sickle erythrocytes target cytotoxics to hypoxic tumor microvessels and potentiate a tumoricidal response. *PLoS one* **8**, e52543
87. Crow, J. P. (1997) Dichlorodihydrofluorescein and dihydrorhodamine 123 are sensitive indicators of peroxynitrite *in vitro*: Implications for intracellular measurement of reactive nitrogen and oxygen species. *Nitric oxide* **1**, 145–157
88. Amer, J., Goldfarb, A., and Fibach, E. (2003) Flow cytometric measurement of reactive oxygen species production by normal and thalassaemic red blood cells. *Eur. J. Haematol.* **70**, 84–90
89. Amer, J., Goldfarb, A., and Fibach, E. (2004) Flow cytometric analysis of the oxidative status of normal and thalassemic red blood cells. *Cytometry A: J. Int. Soc. Anal. Cytol.* **60**, 73–80
90. Parayath, N., Stephan, S., Koehne, A., Nelson, P., and Stephan, M. (2020) *In vitro*-transcribed antigen receptor mRNA nanocarriers for transient expression in circulating T cells *in vivo*. *Nat. Commun.* **11**, 1–17
91. Busino, L., Bassermann, F., Maiolica, A., Lee, C., Nolan, P. M., Godinho, S. I., Draetta, G. F., and Pagano, M. (2007) SCFFbxl3 controls the oscillation of the circadian clock by directing the degradation of cryptochrome proteins. *science* **316**, 900–904
92. Doi, R., Oishi, K., and Ishida, N. (2010) CLOCK regulates circadian rhythms of hepatic glycogen synthesis through transcriptional activation of Gys2. *J. Biol. Chem.* **285**, 22114–22121
93. Travnickova-Bendova, Z., Cermakian, N., Reppert, S. M., and Sassone-Corsi, P. (2002) Bimodal regulation of mPeriod promoters by CREB-dependent signaling and CLOCK/BMAL1 activity. *Proc. Natl. Acad. Sci. U. S. A.* **99**, 7728–7733
94. Gonzalez-Cuyar, L. F., Perry, G., Miyajima, H., Atwood, C. S., Riveros-Angel, M., Lyons, P. F., Siedlak, S. L., Smith, M. A., and Castellani, R. J. (2008) Redox active iron accumulation in Aceruloplasminemia. *Neuropathology* **28**, 466–471
95. Smith, M. A., Harris, P. L., Sayre, L. M., and Perry, G. (1997) Iron accumulation in Alzheimer disease is a source of redox-generated free radicals. *Proc. Natl. Acad. Sci. U. S. A.* **94**, 9866–9868
96. Beckonert, O., Keun, H. C., Ebbels, T. M., Bundy, J., Holmes, E., Lindon, J. C., and Nicholson, J. K. (2007) Metabolic profiling, metabolomic and metabonomic procedures for NMR spectroscopy of urine, plasma, serum and tissue extracts. *Nat. Protoc.* **2**, 2692
97. Braunstein, M., Rose, A. B., Holmes, S. G., Allis, C. D., and Broach, J. R. (1993) Transcriptional silencing in yeast is associated with reduced nucleosome acetylation. *Genes Dev.* **7**, 592–604
98. Spencer, V. A., Sun, J.-M., Li, L., and Davie, J. R. (2003) Chromatin immunoprecipitation: A tool for studying histone acetylation and transcription factor binding. *Methods* **31**, 67–75
99. Zhou, Y. F., Wu, X. M., Zhou, G., Mu, M.d., Zhang, F. L., Li, F. M., Qian, C., Du, F., Yung, W. H., and Qian, Z. M. (2018) Cystathionine β-synthase is required for body iron homeostasis. *Hepatology* **67**, 21–35